*Progress In Electromagnetics Research C, Vol. 97, 1–13, 2019*

# Tunable Multiband Balanced Bandstop Filter with High CMRR

**Dubari Borah and Thottam S. Kalkur***

**Abstract**—A novel and effective architecture of tunable multiband balanced bandstop filter (MBBSF) is introduced for the first time in this paper. Each symmetrical bisection of the proposed branch line structure consists of K series cascaded tunable N-band sections to realize a reconfigurable K-th order N-band response in differential mode (DM) operation. The main advantage lies on the fact that all these N bands can be tuned simultaneously or each band independently. Moreover, it maintains a high common mode rejection ratio (CMRR) for all the tuning states by incorporating open stubs in the symmetrical plane of the balanced structure. To validate the proposed topology, a balanced dualband tunable BSF is designed where the two DM stopbands tune in the range of 1.16 GHz–1.29 GHz and 1.6 GHz–1.76 GHz, respectively. The lower and upper bands maintain a constant absolute bandwidth (ABW) of 115 MHz and 135 MHz, respectively, and stopband rejection is better than 20 dB for each band. The fabricated prototype occupies an area of $0.31\lambda_g^2$, and the experimental results show a good agreement with the simulation results.

## 1. INTRODUCTION

The demand for multiband services in modern communication systems is rapidly increasing as they can deal with several communication signals simultaneously. This growing challenge of spectrum management is usually addressed by using cognitive radios [1]. The receiver module in such a radio is often affected by jamming from high power signals. Therefore, a multiband bandstop filter plays a significant role by rejecting any interfering signal in such a system. For example, a dualband bandstop filter is employed in various wireless systems to suppress two unwanted narrowband signals occurring concurrently within a wide bandwidth [2]. Also, it is used to attenuate the undesired double-sideband spectrum of high-power amplifiers and mixers. Furthermore, as the modern wireless system is continuously striving for compact size, it is necessary to employ tunability to multiband bandstop filter. Such a filter eliminates the use of multiple filter banks and provides dynamic isolation to several interfering signals simultaneously in a crowded spectrum environment. In the past years, a variety of tunable elements such as p-n junction varactors, MEMS, and ferroelectric capacitors have been proposed for implementing tunable filters, phase shifters, and voltage-controlled oscillators [3–5].

Recently, balanced filter topology has gained much popularity for the emerging applications in telecommunication because of its higher noise immunity than the single-ended counterpart. So far, many articles have been found to concentrate on balanced bandpass filter with different characteristics such as ultra-wideband, narrowband, tunable, dualband, high-selectivity and high common mode suppression. However, insertion of a tunable bandpass filter into a communication system cause inevitable insertion loss due to the parasitic resistance associated with the varactors [6]. It gets worse as the resonant frequency moves towards lower value. If a strong interference affecting the desired weak signal is known, bandstop filter is more useful to eliminate the unwanted signal because it can protect the required

*Received 16 April 2019, Accepted 30 October 2019, Scheduled 9 November 2019*
* Corresponding author: Thottam S. Kalkur (tkalkur@uccs.edu).
The authors are with the Microelectronics Research Laboratory, Department of Electrical and Computer Engineering, University of Colorado, Colorado Springs, CO 80918-7150, USA.

signal from significant insertion loss compared to a bandpass filter. Nevertheless, there is only a limited literature available in the field of balanced bandstop filter. In [1] and [6], CM noise of a single-band tunable balanced BSF is suppressed by using magnetic field property of Substrate Integrated Waveguide (SIW) resonators and balanced properties of double-sided parallel-strip line (DSPSL), respectively. The design procedure of each of these two designs is very complex. A differential BSF for a directional filter is reported in [7], which consists of one quarter wavelength coupled line section having coupled and isolated ports terminated in short and open, respectively. In [8], a narrowband balanced BSF design consisting of four coupled-line sections with open-circuited stubs, two half-wavelength transmission lines and two ground resistors is reported. None of these designs give flexibility to extrapolate the single-band response to multiband response. In [9], a single-ended multiband tunable BSF structure is proposed. However, to the best of the authors' knowledge, no differential structure has been published yet which incorporates an arbitrary number of reconfigurable stopbands.

This paper investigates a K-th order N-band reconfigurable balanced BSF structure which offers flexibility to tune all the stopbands simultaneously or to tune each stopband independently. Also, each stopband maintains constant absolute bandwidth (ABW) for the whole tuning range. The common-mode noise is highly eliminated by employing the properties of stepped impedance resonator (SIR).

The paper is organized as follows. Section 2 analyses the theory behind the proposed topology. Section 3 describes the design methodology with an example of balanced dualband BSF, whereas the fabricated prototype and its characterization results are presented in Section 4 to validate its practical viability. Finally, the important points are summarized as the conclusion in Section 5.

## 2. GENERAL STRUCTURE

The proposed four-port reconfigurable MBBSF is shown in Fig. 1(a), which is ideally symmetric to the horizontal central plane (dotted line). Each symmetric bisection of this branch line structure consists of K identical N-band sections, which are cascaded in series through immittance inverters. In any operational mode, each N-band section consists of $N$ stubs with different lengths $(L_1, L_2, ..., L_N)$, separately coupled to the same non-resonating node (NRN) with immittance inverters. All the immittance inverters are designed at center frequency of the entire spectral range of the filter response. Both symmetric bisections are connected through variable capacitors (C) in the symmetry plane for tunability. In this plane, each NRN-NRN' pair also shares an open stub (OS) to suppress the CM noise.

### 2.1. Differential Mode (DM) Operation

When the circuit in Fig. 1(a) is excited by a differential signal, the horizontal central plane acts as a perfect electric wall, i.e., electrically short. Therefore, the open stubs in this plane have no effect on the DM resonant frequencies and their corresponding couplings from the NRNs become short-circuited. The two-port bisection for this operation is presented in Fig. 1(b) which shows that for a given voltage, the capacitor loaded N stubs represent N quarter wavelength resonators (referred to here as bandpass resonators) to produce a N-band BSF response. Therefore, series cascade of K N-band cells in the circuit produces a K-th order N-band bandstop response in DM operation. Also, it should be noted that the capacitor values become twice of those in Fig. 1(a). The design gives much flexibility to change the bandwidth of each stopband. For any band, a wide bandwidth can be realized by increasing the characteristic impedance of the associated resonator or decreasing the characteristic impedance of the inverter connecting that resonator to the NRN.

The basic building block of this DM equivalent circuit is shown in Fig. 2. Here, the short-circuited coupling (Kos) has no effect on the stopband resonant frequencies. Therefore, the multiband frequency transformation compatible with this N-band DM cell is given by [9]:

$$\Omega_{\mathrm{MBBSF}}(f) = -\sum_{i=1}^{N} \frac{1}{\frac{1}{\Delta_i}\left(\frac{f}{f_i} - \frac{f_i}{f}\right)} \tag{1}$$

where $\Omega$ is the normalized lowpass frequency; $f$ is the frequency variable, $f_i$ and $\Delta_i$ are the center frequency and bandwidth scaling factor of the $i$th stopband, respectively. Here, $N$ resonators $L_1$, $L_2$,

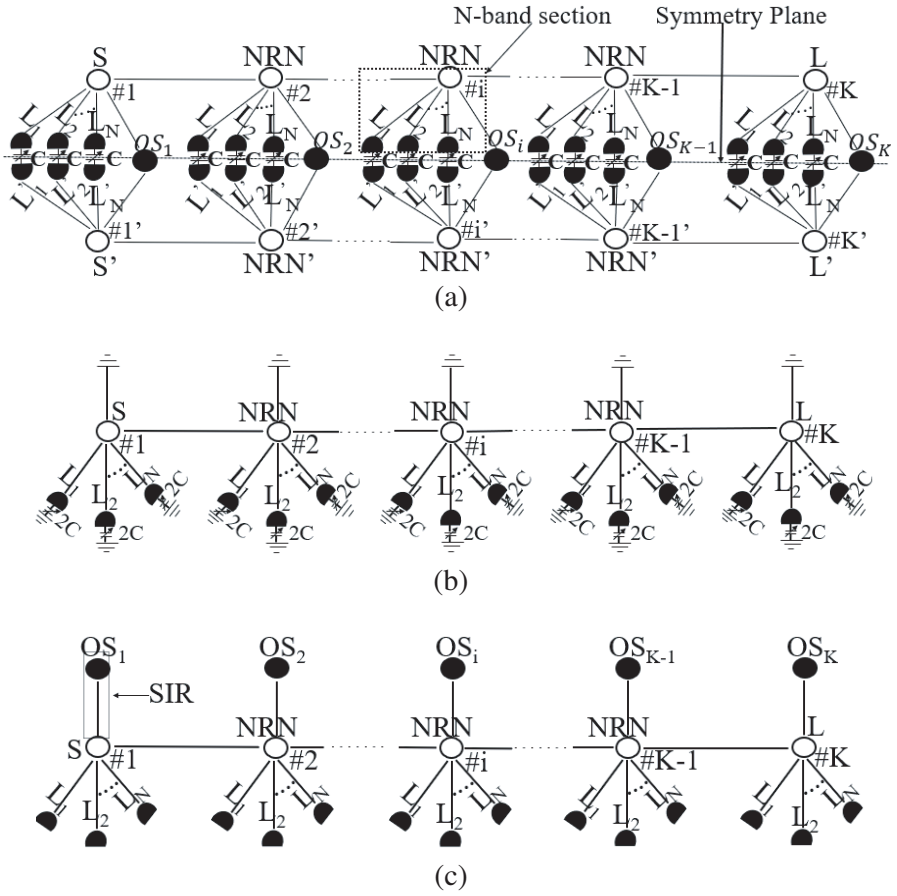


**Figure 1.** (a) Proposed reconfigurable MBBSF, (b) differential mode (DM) equivalent circuit and (c) common mode (CM) equivalent circuit. Here, the black lines denote the immittance inverters between different nodes and the black half circles are $N$ quarter wavelength lines at $N$ frequencies $(L_1, L_2, ..., L_N)$. White full circles represent source (S), load (L) or any other NRNs (or NRN's) whereas black full circles represent open stubs ($OS_1$, $OS_2$, ..., $OS_K$).

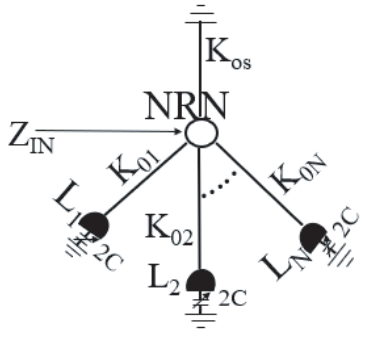


**Figure 2.** N-band cell in DM equivalent circuit.

..., $L_N$) are coupled to the NRN with couplings $K_{oi}$ $(i = 1, 2, ..., N)$. If the frequency offsets are denoted by reactances $X_i$, and the reactance of the short-circuited coupling $(K_{0s})$ is $X_{0s}$, the mathematical expression for input impedance $\{Z_{INi}\}$ $(i = 1, 2, ..., N)$ looking into the NRN at resonance $\{f_i\}$ is given

by,

$$\sum_{i=1}^{N} Z_{INi}(f_i) = \sum_{i=1}^{N} 1/\left(\left(jX_i/K_{0i}^2\right) + \left(1/jX_{0s}\right)\right) = 0 \tag{2}$$

By cascading $K$ number of these building blocks in series, a $K$-th order N-band BSF response can be realized.

In addition to directly generating multiple DM stopbands, this topology has two other advantages when it comes to the tunable response. In a conventional constant absolute bandwidth (ABW) filter where a mix of electric and magnetic couplings are used among the resonators, it is difficult to maintain the tuned center frequency dependence of the couplings uniform throughout the filter [10]. It deteriorates the filter transfer function with tuning. In the proposed topology, all the bandpass resonators are coupled only once to the identical NRNs, allowing all couplings to have identical tuned frequency dependence. The resonator-to-NRN couplings can be designed to have the desired bandwidth versus tuned frequency profile and the filter will be naturally matched within the tuning range provided the stopbands are situated close to each other. The relationship between the external quality factor, $Q_{ex}$ and the ABW is given by Eq. (3) where $M_{1i}$ is the normalized coupling between node 1 and the ith resonator. It shows that $Q_{ex}$ should increase as the frequency shifts upward to achieve a constant ABW [11].

$$Q_{ex} = 1/\left(\text{FBW} \cdot M_{1i}^2\right) = f_i/\left(\text{ABW} \cdot M_{1i}^2\right) \tag{3}$$

The other benefit comes from the fact that the resonators connected to each NRN are parallel to each other. It provides the ability to tune all the stopbands simultaneously or to tune each stopband independently. The input impedance (or reactance) of any isolated tunable bandpass resonator used in the design is zero at resonance. Therefore, the resonant frequency of a varactor loaded bandpass resonator at a given voltage is given by,

$$f_i = 1/\left(2 \cdot \pi \cdot C_i \cdot Z_i \cdot \tan\theta_i(f_i)\right) \tag{4}$$

where $C_i$, $Z_i$, and $\theta_i(f_i)$ are the capacitance, characteristic impedance, and electrical length of the transmission line segment of the $i$th tunable resonator at $f_i$.

### 2.2. Common Mode (CM) Operation

During CM operation, the symmetry plane acts as a perfect magnetic wall, i.e., electrical open circuit. The two-port bisection for this operation is demonstrated in Fig. 1(c) which shows that the capacitors in this plane have no effect on the CM response. However, the open stubs at the central plane provide flexibility to reshape the CM response by extending and reconstructing their couplings from the corresponding NRNs. Each open stub and its coupling from the NRN form a stepped impedance resonator (SIR) under CM operation. At resonance, each SIR produces two transmission zeros (TZs), and the locations of these TZs are determined by the impedance ratio and length ratio of the SIR's constituent line sections. If the two line sections with electrical lengths $\theta_1$ and $\theta_2$ have the characteristic impedances of $Z_1$ and $Z_2$, then total length $\theta_T$ of the SIR is given by Eq. (5) [12, 13],

$$\begin{aligned} \theta_T &= \theta_1 + \theta_2 = \theta_1 + \arctan\frac{Z_2/Z_1}{\tan\theta_1} \\ \text{or} \quad \theta_T &= \theta_1 + \theta_2 = \arctan\frac{Z_2/Z_1}{\tan\theta_2} + \theta_2 \end{aligned} \tag{5}$$

Therefore, if the coupling of any open stub from an NRN is known, the length and characteristic impedance of the open stub can be adjusted in such a way that maximum noise rejection can be achieved for the entire tuning range of each DM stopband. It is not necessary for each NRN-NRN' pair to share an open stub. However, the number of these open stubs should be selected in such a way that for each differential stopband, the CM insertion loss (Scc21) shows an almost 0 dB flat bandpass response to maximize the CMRR value. CMRR is given by the following equation,

$$\text{CMRR} = |\text{Sdd21 (dB)}| - |\text{Scc21 (dB)}| \tag{6}$$

The extraction of all elements in Fig. 1(a) will be discussed in the following section, starting with an example of dualband balanced bandstop filter.

## 3. DESIGN EXAMPLE

To illustrate the proposed topology, first let us consider a second order dualband balanced BSF with DM stopband specifications — $f_1 = 1.16\,\text{GHz}$, $\text{ABW}_{f1} = 115\,\text{MHz}$, $f_2 = 1.6\,\text{GHz}$, $\text{ABW}_{f2} = 135\,\text{MHz}$. In the design process, the first step is to extract the DM equivalent circuit by applying Eq. (1) to a standard two-pole lowpass prototype. This DM two-port circuit is shown in Fig. 3(a) where $\theta$ and $Z$ are length variable and characteristic impedance variable, respectively. Resonator $L_1$ and Resonator $L_2$ are quarter wavelength long at $f_1$ and $f_2$, respectively whereas all the inverters are about quarter wavelength long at $(f_1 + f_2)/2$. The element values in Fig. 3(a) are calculated using Equations (7)–(9) where $g_0$–$g_3$ are element values of the lowpass prototype, $\Delta_1$ and $\Delta_2$ are fractional bandwidths (FBW) of the lower band and upper band respectively [11, 14–16]. In Fig. 3(b), two short-circuited quarter wavelength lines are connected to the NRNs 1 and 2. Their impedances are selected in such a way that Eq. (2) is satisfied, and they don not affect the DM response of the filter.

$$K_{12} = \frac{Z_0}{\sqrt{g_0 \cdot g_3}} \tag{7}$$

$$Z_{L1} = \frac{\sqrt{\pi \Delta_1 g_1}}{2J_{01}} \tag{8}$$

$$Z_{L2} = \frac{\sqrt{\pi \Delta_2 g_2 g_3}}{2J_{02}} \tag{9}$$

These equations can be generalized to realize the elements of the $K$-th order N-band DM equivalent circuit in Fig. 1(b) as follows.

$$K_{j-1,\,j} = \frac{Z_0}{\sqrt{g_0 \cdot g_{K+1}}} \tag{10}$$

$$Z_{Li} = \frac{\sqrt{\pi \Delta_i g_j}}{2J_{0i}} \quad \text{if } j \text{ is odd}$$

$$\text{Or, } Z_{Li} = \frac{\sqrt{\pi \Delta_i g_j g_{K+1}}}{2J_{0i}} \quad \text{if } j \text{ is even} \tag{11}$$

where $i = 1, 2, ..., N$ and $j = 1, 2, ..., K$.

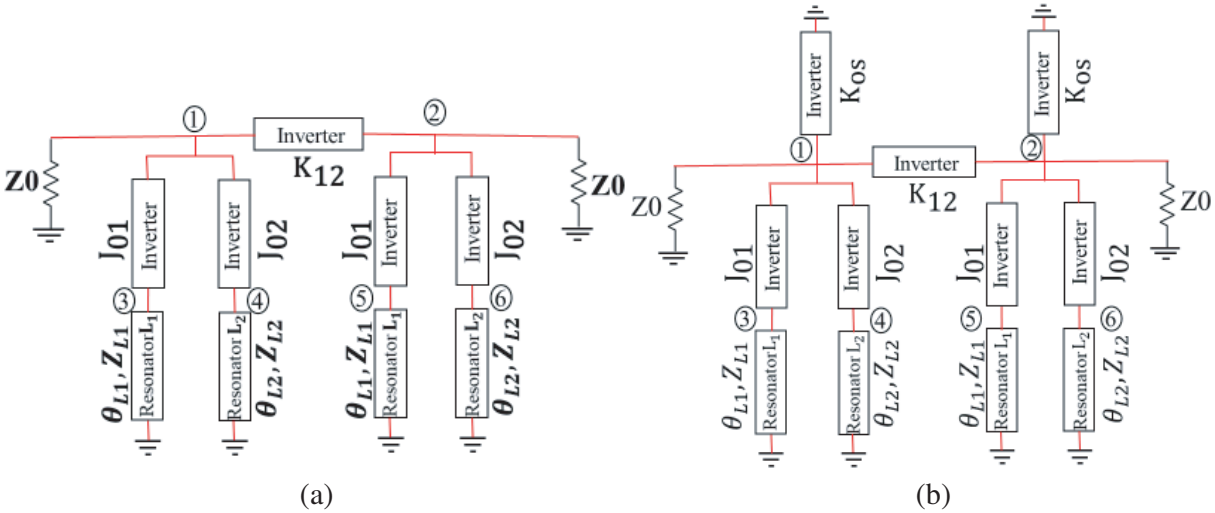


**Figure 3.** (a) Second order dualband network realized from two-pole lowpass prototype. (b) Two short-circuited quarter wavelength stubs are connected to the NRNs 1 and 2 to complete the DM equivalent circuit, without affecting the dualband response.

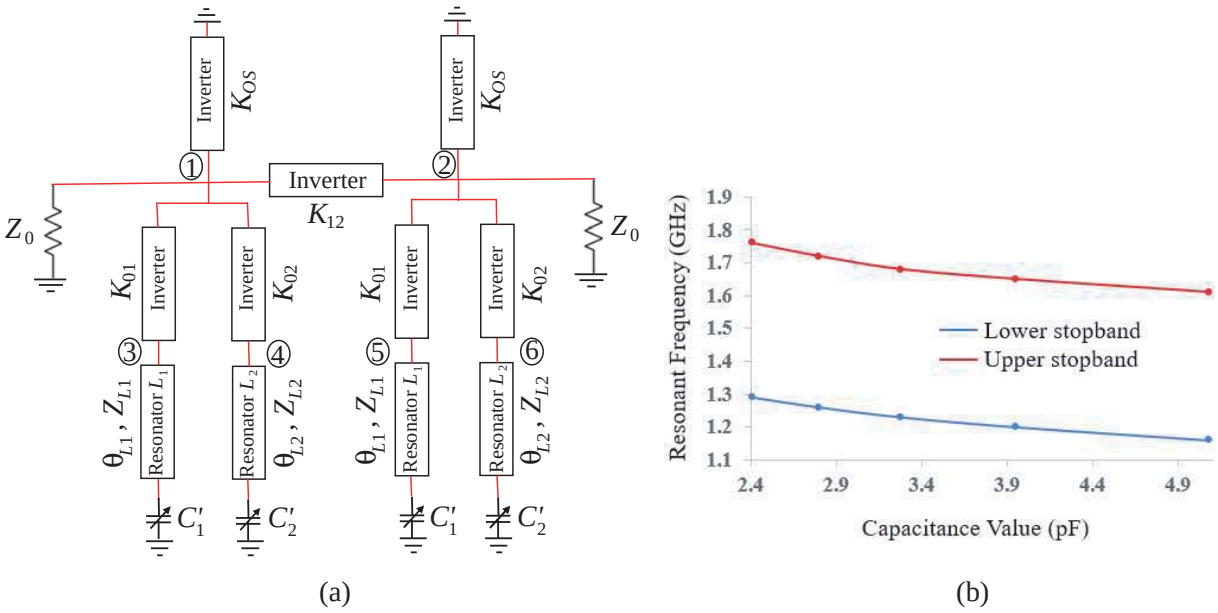


**Figure 4.** (a) Varactor added 2nd order tunable dualband DM equivalent circuit where 1 & 2 are NRNs and 3, 4, 5 & 6 are resonating nodes. (b) Variation of resonant frequency with variable capacitance.

Using Eqs. (7)–(9), the line characteristic impedances of the second order dualband DM equivalent circuit are selected as $Z_{L1} = Z_{L2} = 22\,\Omega$, $J_{01} = J_{02} = 0.0125$ mho and $K_{12} = 50\,\Omega$. Also, $K_{os}$ is selected as $90\,\Omega$ so that it satisfies Eq. (2). The tunable response is achieved by loading each resonator with varactor. Fig. 4(a) shows resonators $L_1$ and $L_2$ are loaded with varactors $C_1^{'}$ and $C_2^{'}$ to control the lower band and the upper band respectively. Based on Eq. (4), the center frequency shifting of each stopband vs. capacitance value is depicted in Fig. 4(b). As the capacitance increases, the stopband resonant frequency goes down.

Figure 5 presents four different simulation results by applying the multiband transformation in Eq. (1) with different sets of design variables. In Fig. 5(a), an example DM dualband response is depicted with design parameters $\Delta_1 = 0.1$, $\Delta_2 = 0.08$, $f_1 = 1.16$ GHz and $f_2 = 1.6$ GHz. Fig. 5(b) shows the tuning of both stopbands with $\Delta_1 = 0.1$, $\Delta_2 = 0.08$ but for #1, $f_1 = 1.16$ GHz, $f_2 = 1.6$ GHz and for #2, $f_1 = 1.29$ GHz, $f_2 = 1.76$ GHz. Fig. 5(c) shows the upper band tuning with design specifications $\Delta_1 = 0.1$, $\Delta_2 = 0.08$, $f_1 = 1.29$ GHz but $f_2 = 1.6$ GHz for #1 whereas $f_2 = 1.76$ GHz for #2. Fig. 5(d) demonstrates the lower band tuning with design variables $\Delta_1 = 0.1$, $\Delta_2 = 0.08$, $f_2 = 1.64$ GHz but $f_1 = 1.16$ GHz for #1 and $f_1 = 1.29$ GHz for #2. Table 1 shows the elements of the $6 \times 6$ matrix associated with different DM filter responses in Fig. 5.

From this normalized coupling matrix, the actual or denormalized coupling coefficient is calculated

**Table 1.** Coupling matrix elements for different filter responses.

| | Fig. 5(a) | Fig. 5(b) | | Fig. 5(c) | | Fig. 5(d) | |
|---|---|---|---|---|---|---|---|
| | | #1 | #2 | #1 | #2 | #1 | #2 |
| $M_{12}$ | 1.1 | 1.1 | 1.1 | 1.1 | 1.1 | 1.1 | 1.1 |
| $M_{13} = M_{25}$ | 0.97 | 0.97 | 0.97 | 0.97 | 0.97 | 0.97 | 0.97 |
| $M_{14} = M_{26}$ | 0.97 | 0.97 | 0.97 | 0.97 | 0.97 | 0.97 | 0.97 |
| $M_{33} = M_{55}$ | 3 | 3 | 3.6 | 3 | 4.4 | 3.6 | 2.3 |
| $M_{44} = M_{66}$ | $-3$ | $-3$ | $-3.6$ | $-3$ | $-4.4$ | 3.6 | $-2.9$ |
| $M_{15} = M_{16} = M_{23} = M_{24}$ | 0 | 0 | 0 | 0 | 0 | 0 | 0 |

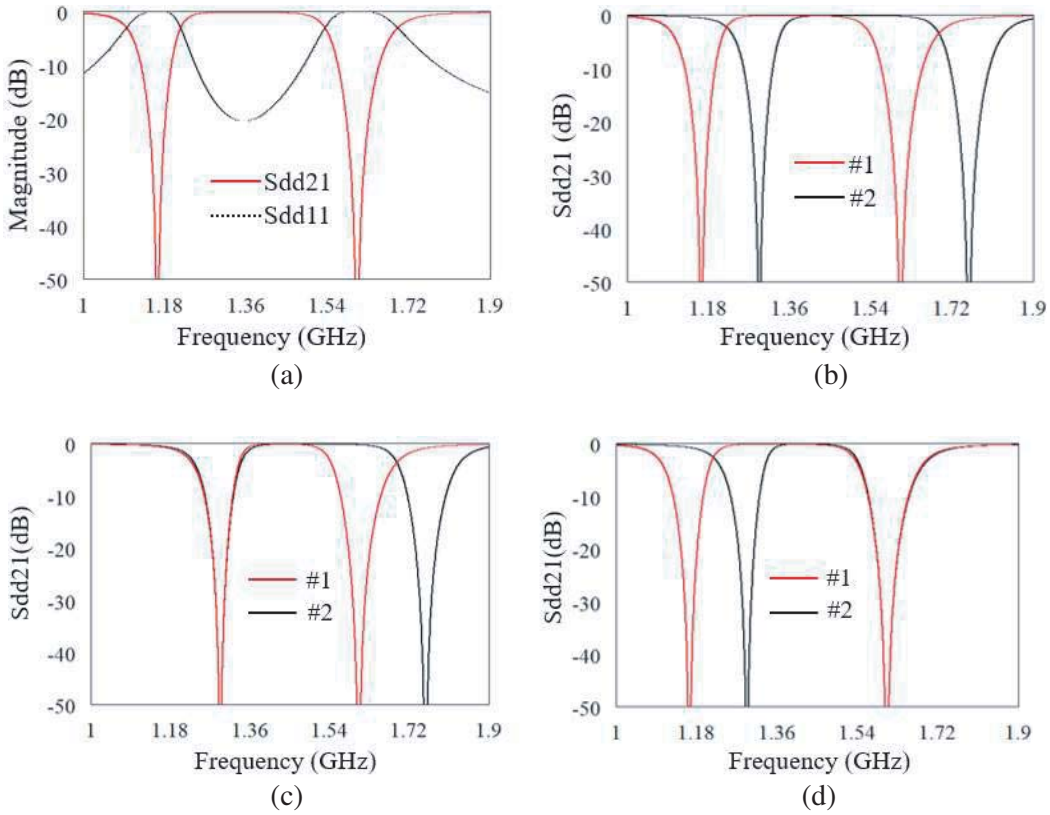


**Figure 5.** (a) Example dualband response showing DM insertion loss (Sdd21) and DM return loss (Sdd11). (b) Sdd21 plot from tuning of both stopbands. (c) Sdd21 plot for independent tuning of upper band. (d) Sdd21 plot for independent tuning of lower band. For all tunable responses, two different states are represented as #1 and #2.

using Eq. (12) where $M_{ij}$ is any element of coupling matrix shown in Table 1 [11, 17].

$$m_{ij} = \text{FBW} \times M_{ij} \tag{12}$$

Similarly, normalized external quality factor is calculated as $q_{ex} = \text{FBW} \times Q_{ex}$ where $Q_{ex}$ is calculated using Eq. (3). The $Q_{ex}$ for this tunable dualband differential design is discussed in detail in the next section.

In CM operation, resonators $L_1$ and $L_2$ of the DM equivalent circuit are no longer short-circuit, rather they are electrically open. Therefore, they cannot produce the two stopbands. Moreover, the stubs with characteristic impedance $K_{os}$ are connected to two open stubs, rather being short-circuit. Each of these stubs is selected to be 40° long at center frequency of the entire spectral range with a characteristic impedance of 24 Ω. Fig. 6 demonstrates how these open stubs control the CM response. Without the open stubs, the Scc21 varies from 0 to 25 dB within the DM tuning ranges whereas with these open stubs, the Scc21 plot shows a flat 0 dB bandpass response, representing a high CMRR.

After extracting both DM and CM equivalent circuits, the complete second order dualband tunable differential filter is shown in Fig. 7. It should be noted that $C_1$ and $C_2$ values for this circuit are half of $C_1'$ and $C_2'$ in Fig. 4, respectively. Similarly, impedances of the open stubs become half of the those in Fig. 6.

## 4. DESIGN VALIDATION

For demonstration, a microstrip-line prototype of the above mentioned dualband balanced tunable BSF is built on Rogers RO4003 with substrate thickness of 1.52 mm, dielectric constant of 3.38 and loss

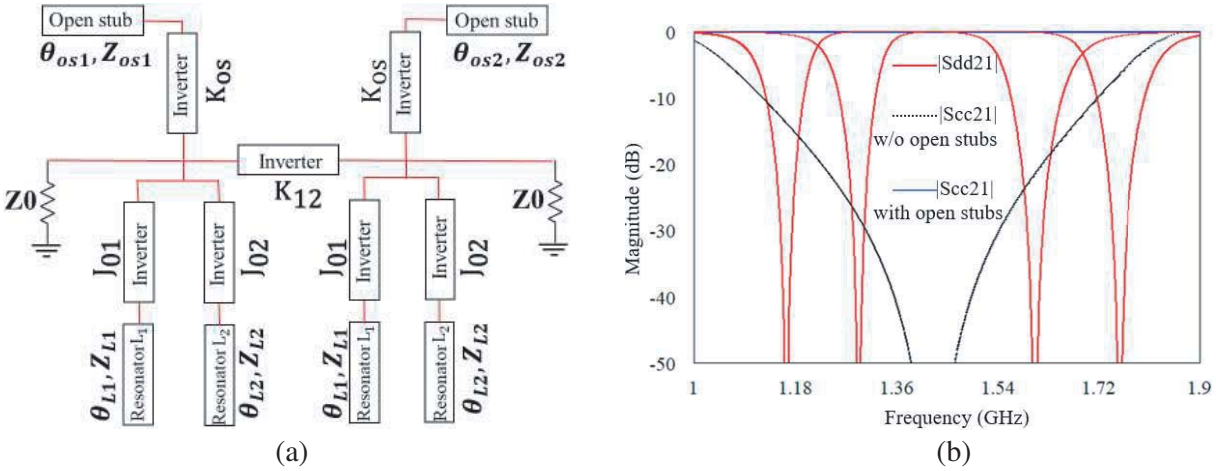


**Figure 6.** (a) CM equivalent circuit of the dualband differential filter and (b) effect of open stubs on CM insertion loss (Scc21).

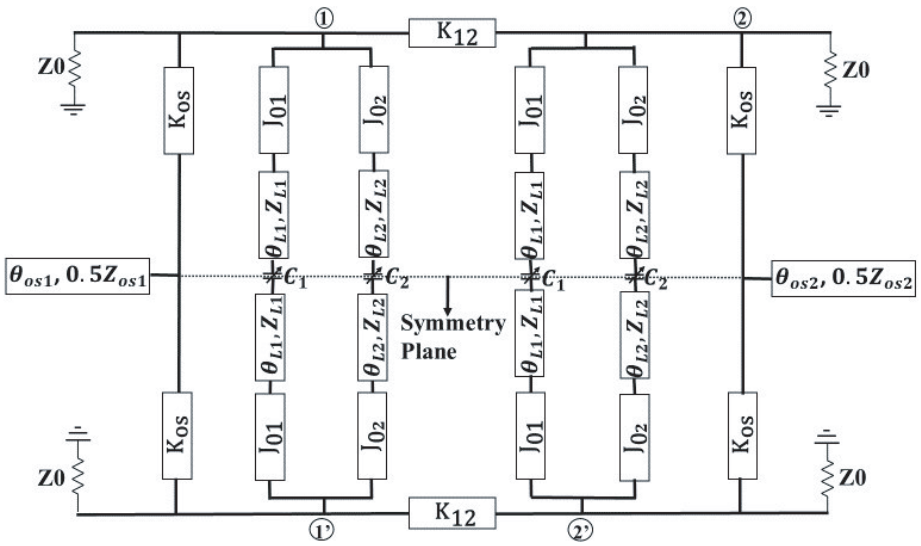


**Figure 7.** Complete circuit of second order dualband tunable differential filter where 1, 1′, 2, 2′ are NRNs.

tangent of 0.0027 (Fig. 8). Further miniaturization can be achieved by implementing all the immittance inverters using lumped elements, multilayer technique, open-loop ring resonators or defected ground structure (DGS) slots as discussed in [18–21]. All the immittance inverters used as the couplings in the design are quarter wavelength long at 1.45 GHz, which is the center frequency of overall spectral range of the designed balanced dualband tunable BSF. Two small 50 Ω transmission line sections (about 4 mm) are connected to the source and load to take care of the external quality factors. The quarter wavelength lines $(\theta_{L1}, Z_{L1})$ and $(\theta_{L2}, Z_{L2})$ which correspond to two DM stopbands are implemented as their equivalent low pass $\pi$ networks [18]. The $\pi$ network for $(\theta_{L1}, Z_{L1})$ consists of a series inductance of 6.2 nH (Coilcraft 0402CS series) and two shunt capacitances of 3.3 pF (Johanson 0402 series) each. Similarly, the $\pi$ network for $(\theta_{L2}, Z_{L2})$consists of a series inductance of 3.9 nH (Coilcraft 0402CS series) and two shunt capacitances of 2.4 pF (Johanson 0402series) each. Dimensions of the other line sections are shown in the figure. For the varactors, Skyworks SMV1233 model is used. The dc bias voltage to the varactors was applied through the input ports (port 1 and port 1′) of the filter using two built in bias tees inside the network analyzer. In case of independent control of any stopband, Johanson 0402

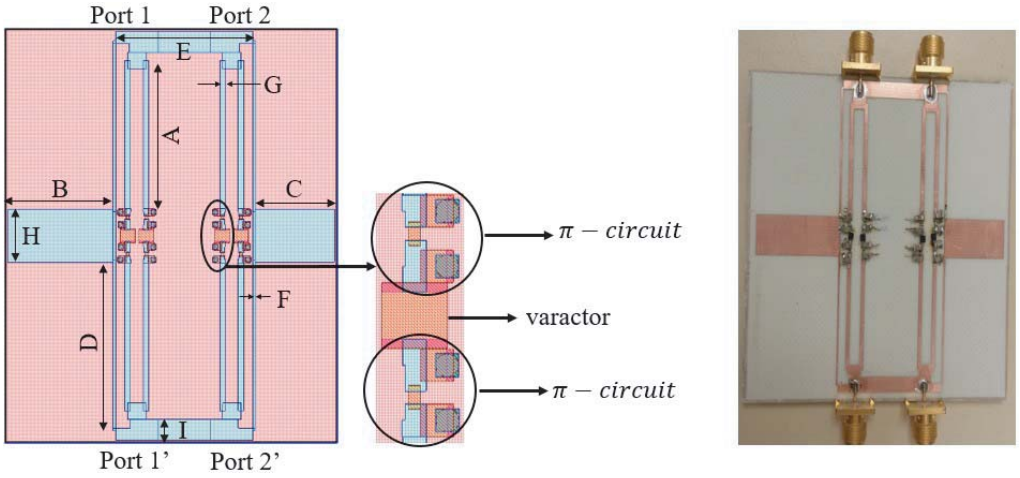


**Figure 8.** (a) Layout with zoomed version of central portion showing varactor and LC $\pi$-circuits. $\pi$-circuit is used to replace each of $(\theta_{L1}, Z_{L1})$ and $(\theta_{L2}, Z_{L2})$ in Fig. 7. $A$ = immittance inverter length, connected to each $\pi$-circuit = 28 mm; $B$ = left openstub length = 20 mm; $C$ = right open stub length = 15 mm; $D$ = immittance inverter length, connected to each open stub = 32 mm; $E$ = Separation between two open stubs = 26 mm; $F$ = immittance inverter width, connected to each open stub = 0.5 mm; $G$ = immittance inverter width, connected to each $\pi$-circuit = 1 mm; $H$ = each open stub width = 10 mm, $I$ = immittance inverter width between two dualband sections = 4 mm and (b) photograph of the fabricated model.

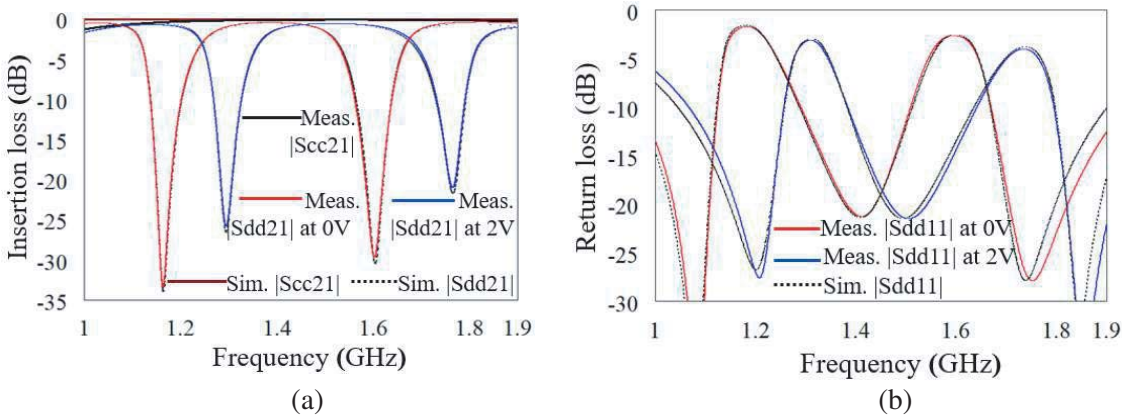


**Figure 9.** Simulated and measured results from simultaneous tuning of both stopbands. (a) DM insertion loss (Sdd21) and CM insertion loss (Scc21). (b) DM return loss (Sdd11).

series is used for the static capactiors in the symmetry plane. Simulation is done in NI/AWR Microwave Office and characterization is performed with the help of Keysight N5224 4-port PNA.

Figure 9 illustrates the center frequency agility of both stopbands. The lower band tunes in the range of 1.16 GHz–1.29 GHz whereas tuning range of the upper band is 1.6 GHz–1.76 GHz. The rejection level of the lower band varies from 33 dB to 25.7 dB and that for the upper one changes from 30 dB to 21 dB. It should be also noted from Fig. 9(b) that maximum possible spectral separation between the two stopbands is constrained by the deterioration of the in-band return loss [10]. For this circuit with the given bandwidth states, an upper to lower frequency ratio of 1.36 to 1.38 (i.e., 440 MHz–470 MHz) can be achieved for a maximum return loss level of about 4 dB. Table 2 demonstrates that the ABWs for both stopbands show a small shift of 7 MHz within their respective tuning ranges. This is because

**Table 2.** Variation of absolute bandwidths (ABW) as both stopbands tune.

| Tuning state # | Lower stopband center frequency (GHz) | ABW (MHz) | Upper stopband center frequency (GHz) | ABW (MHz) |
|---|---|---|---|---|
| 1 | 1.16 | 115 | 1.60 | 135 |
| 2 | 1.20 | 114 | 1.65 | 135 |
| 3 | 1.23 | 112 | 1.68 | 133 |
| 4 | 1.26 | 110 | 1.72 | 130 |
| 5 | 1.29 | 108 | 1.76 | 129 |

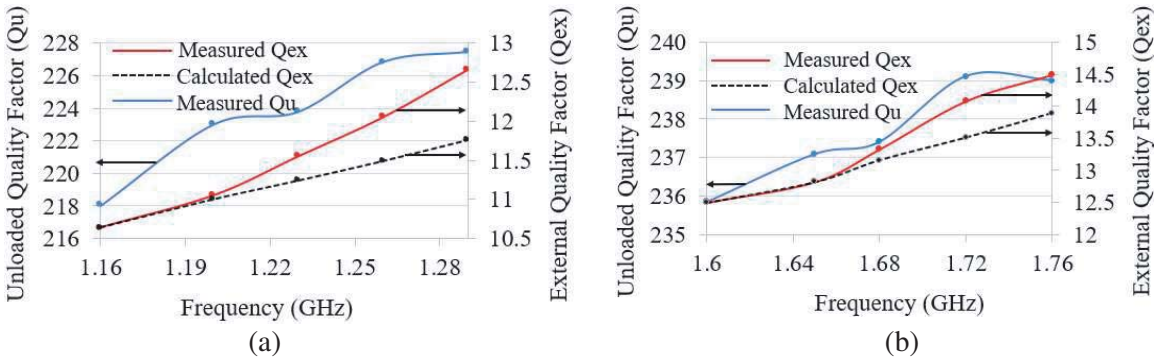


**Figure 10.** Unloaded and external quality factors associated with (a) resonator $L1$ and (b) resonator $L2$.

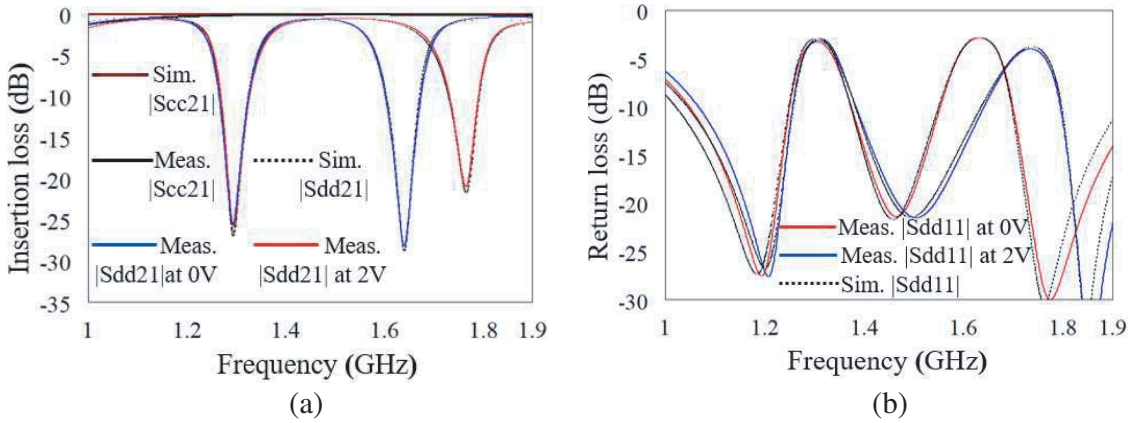


**Figure 11.** Simulated and measured results from independent tuning of upper band where $C1 = 2.5$ pF. (a) DM insertion loss (Sdd21) and CM insertion loss (Scc21). (b) DM return loss (Sdd11).

the reconfiguration process slightly alters the existing couplings in the design. Fig. 10 demonstrates how the unloaded quality factor $Q_u$ and external quality factor $Q_{ex}$ for both resonators vary with frequency. Under higher bias voltage, the varactors exhibit lower series resistance which results in $Q_u$ enhancement with frequency. Also, from Eq. (3), the $Q_{ex}$ of each resonator shows an expected increasing trend with frequency to keep the ABW almost constant.

Figure 11 shows the center frequency tuning of the upper stopband. It tunes from 1.64 GHz to 1.76 GHz whereas the lower one stays fixed at 1.29 GHz. The 3-dB bandwidth for the upper band falls in the range of 128 MHz–136 MHz, with a power rejection of greater than 20 dB within the tuning range.

Similarly, Fig. 12 demonstrates the center frequency agility of the lower band. It tunes from

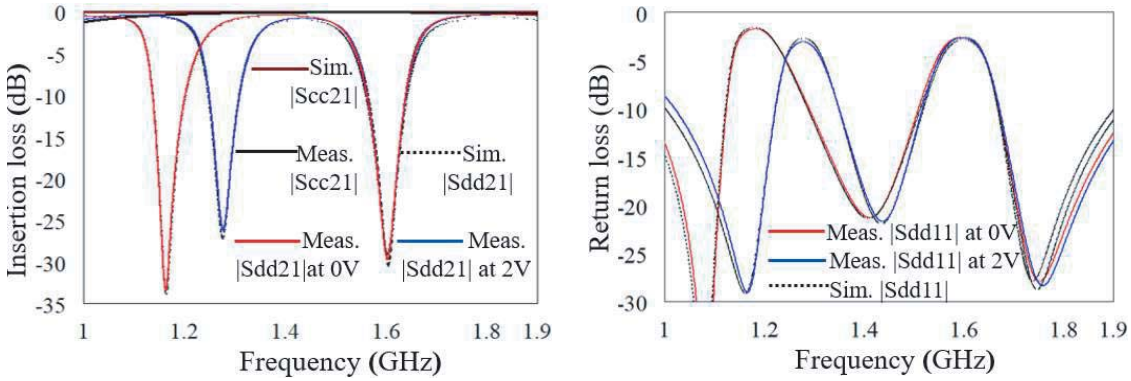


**Figure 12.** Simulated and measured results from independent tuning of lower stopband where $C2 = 5$ pF. (a) DM insertion loss (Sdd21) and CM insertion loss (Scc21). (b) DM return loss (Sdd11).

**Table 3.** Comparison of different balanced bandstop filter designs.

| Parameters | [1] | [6] | [7] | [8] | **This work** |
|---|---|---|---|---|---|
| #Stopbands | 1 | 1 | 1 | 1 | **2(*)** |
| DM center frequencies (GHz) | 1.57 | 0.83 | 2.45 | 2 | **1.22/1.68** |
| Tunability (GHz) | 1.57–3.18 | 0.58–1.07 | – | – | **(1.16–1.29)/(1.6–1.76)** |
| Minimum Sdd21 (dB) | 47 | 10.5 | 15 | 18.89 | **26/21** |
| Maximum Sdd11 (dB) | 0.5 | 8 | - | 2.5 | **4(*)** |
| Scc21 (dB) in 3 dB DM bandwidths | 0 | 13 | 0 | 50.45 | **0** |
| Minimum \|CMRR\| (dB) | 47 | 2.5 | 15 | 31.56 | **26/21** |
| Effective size ($\lambda_g^2$) | 0.14 | 0.09 | – | 0.34 | **0.31** |

$\lambda_g$ denotes guided wavelength at DM center frequency. (*) denotes it can be extrapolated to any number of stopbands and Sdd11 will be reduced for a smaller spectral separation between the two bands.

1.17 GHz to 1.28 GHz while the upper band remains centered at 1.6 GHz. The 3-dB bandwidth of lower band varies in the range of 109 MHz–115 MHz and stopband rejection level is better than 26 dB. Within this tuning range, in band return loss is 2.7 dB or less.

In the case of independent tuning of each stopband, $Q$-factors of the tunable resonator follow the same plot shown in Fig. 10. Finally, Table 3 shows the comparison between the fabricated model using the proposed topology and already published related work. The main advantage of this design over the listed designs lies on the fact that it can incorporate multiple stopbands, and all of them can be reconfigured maintaining constant ABW. Additionally, the bands can be tuned all together or individually, with respect to center frequency. Moreover, the minimum stopband rejection level (Sdd21) and the minimum CMRR value are higher than most of the designs mentioned in the table.

## 5. CONCLUSION

A reconfigurable multiband balanced BSF with high CMRR is presented for the first time in this paper. Each symmetrical bisection of the proposed branch line structure is designed by cascading multiband cells in series through immittance inverters. For center frequency tunability of each DM stopband, variable capacitors are connected to the resonator cells in the symmetry plane whereas CM noise is highly eliminated by employing open stubs in the symmetry plane. As the resonators corresponding

to different bands are in parallel to each other in each multiband cell, it gives flexibility to tune either each frequency band independently or all bands simultaneously. To illustrate the proposed topology, a microstrip line prototype of second order balanced dualband tunable BSF is designed and fabricated with tuning ranges of 1.16 GHz–1.29 GHz for lower band and 1.6 GHz–1.76 GHz for upper band, respectively. It maintains a CMRR value of better than 20 dB for each band by applying two open stubs along the central plane. The fabricated prototype occupies an area of $0.31\lambda_g^2$, and the experimental results show a good agreement with the simulation results.

## REFERENCES


1. Hagag, M. F., M. Abdelfattah, and D. Peroulis, "Balanced octave-tunable absorptive bandstop filter," *2018 IEEE 19th Wireless and Microwave Technology Conference (WAMICON)*, 1–4, Sand Key, FL, 2018.
2. Chen, P., L. Li, K. Yang, K. Hua, and X. Luo, "A microstrip dualband bandstop filter with dualband bandstop resonators," *2017 IEEE 17th International Conference on Communication Technology (ICCT)*, 1685–1688, Chengdu, 2017.
3. Aldeeb, H. and T. S. Kalkur, "A novel tunable dual-band bandstop filter (DBBSF) using BST capacitors and tuning diode," *Progress In Electromagnetics Research C*, Vol. 67, 59–69, 2016.
4. Subramanyam, G., M. Cole, N. Sun, N. Sbrockey, G. S. Tompa, and T. S. Kalkur, "Complex oxide based electronics," *Journal of Applied Physics*, Vol. 114, 191301-1 to 35, 2013.
5. Muhhamad, A., T. S. Kalkur, and N. Cramer, "1 GHz active phase shifter based on tunable high-dielectric constant BST thin films," *IEEE Microwave and Guided Letters*, Vol. 16, 261–263, 2006.
6. Cai, J., Y. J. Yang, W. Qin, and J. X. Chen, "Wideband tunable differential bandstop filter based on double-sided parallel-strip line," *IEEE Transactions on Components, Packaging and Manufacturing Technology*, Vol. 8, No. 10, 1815–1822, 2018.
7. Sorocki, J., I. Piekarz, S. Gruszczynski, and K. Wincza, "Low-loss directional filters based on differential band-reject filters with improved isolation using phase inverter," *IEEE Microwave and Wireless Components Letters*, Vol. 28, No. 4, 314–316, April 2018.
8. Kong, M., Y. Wu, Z. Zhuang, and Y. Liu, "Narrowband balanced absorptive bandstop filter integrated with wideband bandpass response," *Electronics Letters*, Vol. 54, No. 4, 225–227, February 22, 2018.
9. Psychogiou, D., R. Gómez-García, and D. Peroulis, "Fully adaptive multiband bandstop filtering sections and their application to multifunctional components," *IEEE Transactions on Microwave Theory and Techniques*, Vol. 64, No. 12, 4405–4418, December 2016.
10. Gómez-García, R. and A. C. Guyette, "Reconfigurable multi-band microwave filters," *IEEE Transactions on Microwave Theory and Techniques*, Vol. 63, No. 4, 1294–1307, April 2015.
11. Hong, J.-S., *Microstrip Filters for RF/Microwave Applications*, Wiley, Hoboken, NJ, 2011.
12. Sagawa, M., M. Makimoto, and S. Yamashita, "Geometrical structures and fundamental characteristics of microwave stepped-impedance resonators," *IEEE Transactions on Microwave Theory and Techniques*, Vol. 45, No. 7, 1078–1085, July 1997.
13. Chen, F., R. Li, J. Qiu, and Q. Chu, "Sharp-rejection wideband bandstop filter using stepped impedance resonators," *IEEE Transactions on Components, Packaging and Manufacturing Technology*, Vol. 7, No. 3, 444–449, March 2017.
14. Hunter, I. C., *Theory and Design of Microwave Filters*, IEE Press, London, U.K., 2001.
15. Pozar, D. M., *Microwave Engineering*, Wiley, Hoboken, NJ, 2012.
16. Ou, Y. and G. M. Rebeiz, "Lumped-element fully tunable bandstop filters for cognitive radio applications," *IEEE Transactions on Microwave Theory and Techniques*, Vol. 59, No. 10, 2461–2468, Oct. 2011.
17. Boutejdar, A., S. Elhani, and S. D. Bennani, "Design of a novel slotted bandpass-bandstop filters using U-resonator and suspended multilayer-technique for L/X-band and WLAN/WiMAX applications," *2017 International Conference on Electrical and Information Technologies (ICEIT)*, 1–7, Rabat, 2017.

18. Elsbury, M. M., P. D. Dresselhaus, S. P. Benz, and Z. Popovic, "Integrated broadband lumped-element symmetrical-hybrid N-way power dividers," *2009 IEEE MTT-S International Microwave Symposium Digest*, 997–1000, Boston, MA, 2009.
19. Boutejdar, A. and A. Omar, "A miniature 5.2-GHz bandstop microstrip filter using multilayer-technique and coupled octagonal defected ground structure," *Microwave Opt. Technol. Lett.*, Vol. 51, 2810–2813, 2009.
20. Boutejdar, A. and S. Bennani, "Design and fabrication of tri-stopband bandstop filters using cascaded and multi-armed methods," *Advanced Electromagnetics*, Vol. 6, No. 3, 18–24, 2017.
21. Boutejdar, A. and A. Omar, "Miniaturized lowpass and bandstop filters using controlled coupling of open-loop-ring defected ground structure," *Microw. Opt. Technol. Lett.*, Vol. 52, No. 11, 2575–2578, 2010.